Single-molecule orientations determined by direct emission pattern imaging

M. Andreas Lieb, James M. Zavislan, and Lukas Novotny

The Institute of Optics, University of Rochester, Rochester, New York 14627

Received September 2, 2003; revised manuscript received November 12, 2003; accepted January 5, 2004

We demonstrate a new method of determining the three-dimensional dipole orientations of single molecules by direct imaging of the emission patterns in the back focal plane of a high-numerical-aperture objective lens. We compare the reconstructed emission-dipole orientations with a previously established method of absorption-dipole mapping. We find that, for a given number of emitted photons, emission pattern imaging provides better accuracy (1°–2°) than absorption-dipole mapping of single molecules. Compared with some other methods for emission-dipole mapping, the presented method is (1) less sensitive to optical aberrations and adjustment and (2) data analysis is simplified because radiation patterns can be expressed in a simple analytical form.

OCIS codes: 180.2520, 260.2510, 300.2140, 300.2530

1. INTRODUCTION

During the past ten years, single-molecule fluorescence spectroscopy has opened a new window to the nanometer scale. Single-molecule spectroscopy has become an increasingly important technique, particularly for molecular biology (see, e.g., Ref. 1), because it gives access to local physical and chemical properties and because it overcomes the loss of information inherent to ensemble averaging (see, e.g., Ref. 2). Various photophysical parameters of a single molecule depend on the orientation of the molecule's absorption- or emission-dipole moment. Examples are excited-state lifetimes,[3] emission intensity, and energy-transfer rates between molecules. Furthermore, the dipole orientation can be used as a probe for the molecule's photophysics,[4,5] for the properties of its environment,[6] and—most important for molecular biology—for the structure and dynamics of dye-labeled macromolecules.[7]

In the past, different methods have been developed to determine either the two-dimensional projection or the full three-dimensional (3D) orientation of the absorption–emission transition dipole moment. 3D determination of the absorption dipole is accomplished by the recording of the excitation rate of the molecule as it is raster scanned through the inhomogeneous field distribution in a strongly focused beam[8,9] or near a near-field optical probe.[10] Other methods are based on tomographic imaging[11] or excitation polarization modulation.[12] Similarly, the 3D orientation of the emission dipole can be determined by a sophisticated polarization analysis (PA) of the emitted fluorescence[13] or by the recording of the defocused[14,15] or aberrated[16] fluorescence image of the molecule. Here we show that the orientation of the emission dipole is directly encoded in the spatial distribution of the emitted light and that it is possible to uniquely reconstruct the emission-dipole moment from a molecule's emission pattern. We record the emission pattern by collecting the emitted photons with an objective lens and by imaging the intensity distribution in the objective's back focal plane (or the back-aperture plane for an infinity-corrected system). We experimentally implement imaging of the emission pattern by adding a Bertrand lens at the exit port of a regular inverted microscope.

The main difference of our approach from that of other methods of emission-dipole orientation determination (i.e., Refs. 14–16) is that we directly record the emission pattern in the *exit pupil* of the optical system, whereas the other methods use a defocused *image* of the dipole emitter. This makes the proposed method less sensitive to phase aberrations and independent of knowledge of the amount of defocus.

2. THEORY

In free space, the radiation pattern of a dipole is characterized by a $\sin^2\theta$ distribution, where θ is the angle between the dipole axis and the observation direction.[17] However, most high-resolution single-molecule experiments are performed near dielectric interfaces. The photons emitted by a single molecule can scatter at the interface, thereby altering the molecule's emission pattern. Dipole emission near planar interfaces was the subject of various theoretical studies during the twentieth century.[18–24] Sommerfeld had already developed a theory for a perpendicularly oriented dipole in 1909.[18] The horizontally oriented dipole was analyzed in 1911 by one of his students.[19,20] Later, in 1919, Weyl reformulated the problem by using an expansion of plane waves and evanescent waves.[22] The predicted emission patterns were confirmed experimentally in 1984 for an ensemble of molecules, i.e., for averaged dipole orientations.[25]

Here, we consider a single molecule that is placed on the surface of a glass substrate (coverslip) and positioned in the focus of the objective lens. To calculate the intensities in the back-aperture plane of the objective lens we use the Weyl representation[22] and assume an aplanatic system, which is well met by modern high-numerical-aperture (NA) objective lenses. A photon emitted at an angle θ to the optical axis is effectively refracted at the

reference sphere of the objective and then directed onto the back-aperture plane. To conserve the energy along each geometric path, the standard apodization factor $\cos^{-1}\theta$ is introduced. The resulting intensity distribution I in the back aperture can be represented as

$$I(r, \varphi, \Theta, \Phi) \propto \frac{1}{\cos\theta}(E_p E_p^* + E_s E_s^*), \tag{1}$$

where r is the radial distance from the optical axis, φ is the azimuthal angle in the back-aperture plane, and Θ is the polar angle and Φ is the azimuthal angle of the dipole axis (see Fig. 1). Note that $r/f = \sin\theta$, with f denoting the focal length. E_p, E_p^*, E_s, and E_s^* are the p- and the s-polarized components of the electric field and their complex conjugates, given by

$$\begin{aligned} E_p &= [c_1(\theta)\cos\Theta\sin\theta \\ &\quad + c_2(\theta)\sin\Theta\cos\theta\cos(\varphi - \Phi)], \\ E_s &= c_3(\theta)\sin\Theta\sin(\varphi - \Phi), \end{aligned} \tag{2}$$

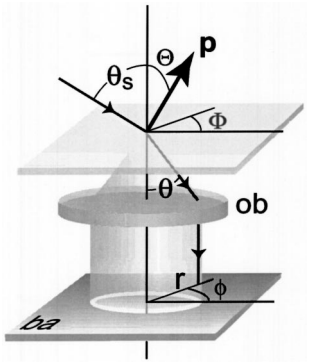

Fig. 1. Coordinate system used for calculations: **p**, dipole moment; ob, the objective lens; ba, the back aperture of the objective lens.

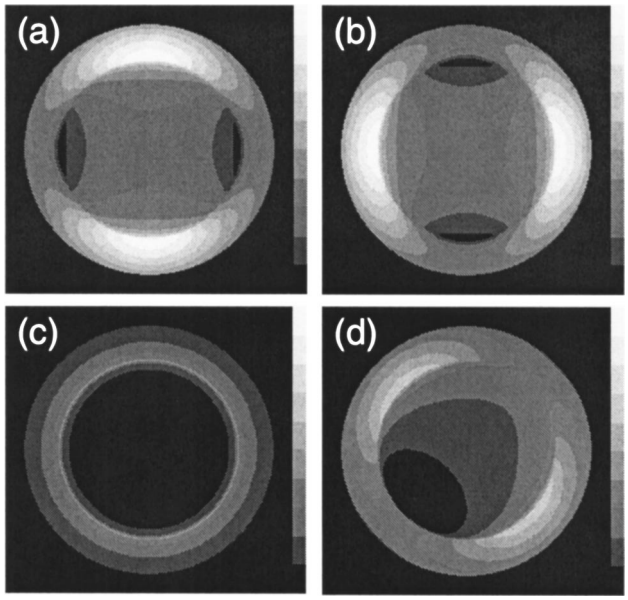

Fig. 2. Calculated emission patterns of a dipole at an air–glass interface ($n_{air} = 1.0$, $n_{glass} = 1.52$) in the back-aperture plane of a NA = 1.4 objective lens: (a) $\Theta = 90°$, $\Phi = 0°$ (horizontal dipole); (b) $\Theta = 90°$, $\Phi = 90°$ (horizontal dipole); (c) $\Theta = 0°$, $\Phi = 0°$ (vertical dipole); (d) $\Theta = 45°$, $\Phi = 45°$.

with c_1, c_2 amd c_3 given by

$$\begin{aligned} c_1(\theta) &= n^2\frac{\cos\theta}{\cos\theta_s}t^p(\theta_s)\Pi(\theta_s), \\ c_2(\theta) &= nt^p(\theta_s)\Pi(\theta_s), \\ c_3(\theta) &= -\,n\frac{\cos\theta}{\cos\theta_s}t^s(\theta_s)\Pi(\theta_s), \\ \Pi(\theta_s) &= \exp(ikn_1\cos\theta_s\delta) \end{aligned} \tag{3}$$

for a dipole above an interface. For a dipole below an interface, they are given by

$$\begin{aligned} c_1(\theta) &= \Pi^{-1}(\theta) + r^p(\theta)\Pi(\theta), \\ c_2(\theta) &= \Pi^{-1}(\theta) - r^p(\theta)\Pi(\theta), \\ c_3(\theta) &= -\,[\Pi^{-1}(\theta) + r^s(\theta)\Pi(\theta)], \\ \Pi(\theta) &= \exp(-ikn_2\cos\theta\delta), \end{aligned} \tag{4}$$

where n is the relative index of refraction n_2/n_1 and t^p, t^s and r^p, r^s are the Fresnel transmission and reflection coefficients for p- and s-polarized light, respectively, as defined in Ref. 26. k is the vacuum wave vector, and δ is the z coordinate of the dipole emitter. Note that θ is allowed to be larger then the critical angle θ_c of the interface, which yields complex-valued θ_s according to Snell's law. The intensity beyond θ_c originates from the conversion of the dipole's near field into propagating fields in the substrate (referred to as forbidden light[27]). Whereas the calculation of aberrated or defocused images of a single dipole emitter involves the solution of rather complicated Fresnel integrals,[28] the calculation of the emission pattern in the back-aperture plane according to Proportion (1) and Eqs. (2) is fairly simple, facilitating data analysis.

In Fig. 2 we show calculated emission patterns for a single molecule with four different dipole orientations. In Figs. 2(a) and 2(b) the molecule is oriented transverse to the optical axis, i.e., its dipole is in the plane of the surface of the supporting substrate. In Fig. 2(c) the dipole axis is vertical to the substrate, and in Fig. 2(d) it is 45 degrees out of the plane of the substrate. The dipole orientations are defined by the angles Θ and Φ, as defined in Fig. 1. The four patterns show distinct differences, making it easy to distinguish among the different dipole orientations, even for poor signal-to-noise ratios (SNR). Most apparent is the discontinuous separation between an inner and an outer region. The boundary between these regions corresponds to the critical angle of total internal reflection ($\theta = \theta_c$) at the air–glass interface. The integrated intensity beyond θ_c (referred to as forbidden light[27]) exceeds the power emitted at angles smaller than θ_c.

3. EXPERIMENT

Our experimental setup (see Fig. 3) consists of a frequency-doubled Nd:YAG laser ($\lambda = 532$ nm) with attached polarization optics, which allows linearly as well as radially polarized excitation.[29] The laser beam is fed into a standard inverted microscope (Nikon TE300). After reflection at a dichroic beam splitter, the light is focused by a high-NA objective (PlanApo 100×, NA = 1.4). The sample, consisting of single molecules deposited on a

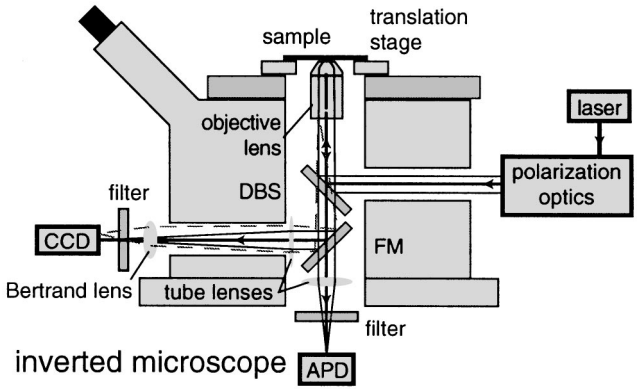

Fig. 3. Experimental setup consisting of an inverted microscope, a green excitation laser ($\lambda = 532$ nm), a polarization optics box containing a half-wave plate, a quarter-wave plate, and a mode converter (see Ref. 29). DBS, dichroic mirror; FM, flip mirror; APD, avalanche photodiode; CCD, a cooled CCD camera.

glass coverslip, is mounted on a closed-loop nanometer-precision piezoelectric scanner that translates the sample in the focal plane (x, y). The emitted fluorescence from the sample is collected by the same objective. We record confocal images of the single-molecule sample by raster scanning the sample and focusing the collected photons onto a single-photon-counting avalanche photodiode (APD in Fig. 3). Assuming a constant absorption cross section and quantum yield, the photon emission rate at each position (x, y) of the sample represents the excitation rate, which depends on the angle enclosed by the *absorption*-dipole axis and the local electric-field vector.[8,9] On the other hand, we determine the orientation of a molecule's *emission* dipole by centering the molecule on the optical axis and imaging the intensity distribution in the back-aperture plane. We accomplish the latter by placing a Bertrand lens ($f = 25$ mm) at the front port of the inverted microscope and projecting the image onto a cooled CCD camera. We adjust the position of Bertrand lens and CCD such that a clear image of the objective's back aperture is recorded. The parameters in our system yield a magnification of $M = 0.27$, i.e., the size of the image on the CCD is 0.27 times the size of the image in the back-aperture plane.

We prepared samples by spincasting 10 μl of a 1-nM solution of 1,1′-dioctadecyl-3,3,3′,3′-tetramethylindocarbocyanine perchlorate [$DiIC_{18}(3)$] in methanol on a clean glass coverslip and by overcoating it with a thin film (10–30 nm) of poly(methyl methacrylate) (PMMA) to improve the photostability of the dye.

We performed data acquisition by first acquiring a scanning confocal image of the sample and identifying the locations of single DiI molecules. After the flip mirror (FM in Fig. 3) was switched to direct the light onto the CCD, individual molecules were positioned into the center of the laser's focal spot. The positioning accuracy is determined by the repeatability of the scan stage and the determination of the location of a molecule from its diffraction-limited image to better than 50 nm. A shutter opened the laser beam path only during data acquisition to prevent photobleaching of the molecules before actual measurements. The CCD was used in a binning mode, in which blocks of 3×3 pixels—corresponding to $78\ \mu$m $\times$ $78\ \mu$m—were binned together to form a superpixel. This results in a single-molecule emission pattern consisting of 13×13 superpixels. To achieve a good SNR of 10–20, we used integration times of 1 s. For observation of faster processes (such as conformational dynamics of proteins), the pixel resolution and the integration time can be noticeably reduced.

4. RESULTS

A typical emission pattern from a single molecule is shown in Fig. 4(a). Each measured emission pattern can be fitted according to Proportion (1) to determine the orientation of the molecule's emission dipole. We obtain our fit function by evaluating Proportion (1) and Eqs. (2) and (4) for a molecule at an air–glass interface on a grid with pixels that have the same size as that of the corresponding superpixels in the experimental images. The theoretical value of each superpixel is the average of 5×5 subpixels. This averaging mimics the integrating character of the CCD, and it accounts for the strong intensity changes near the critical angle and near the rims of the back aperture. Figure 4 shows an example of a measured [Fig. 4(a)] and a fitted [Fig. 4(b)] emission pattern. Cross sections along the horizontal [Fig. 4(c)] and the vertical [Fig. 4(d)] directions are in excellent agreement within the error bounds. The *model* in Figs. 4(c) and 4(d) is directly calculated with Proportion (1), whereas the *fit* corresponds to the discretized 5×5 point-summed values, as mentioned above.

To our best knowledge this is the first time that direct emission patterns of single molecules have been reported,

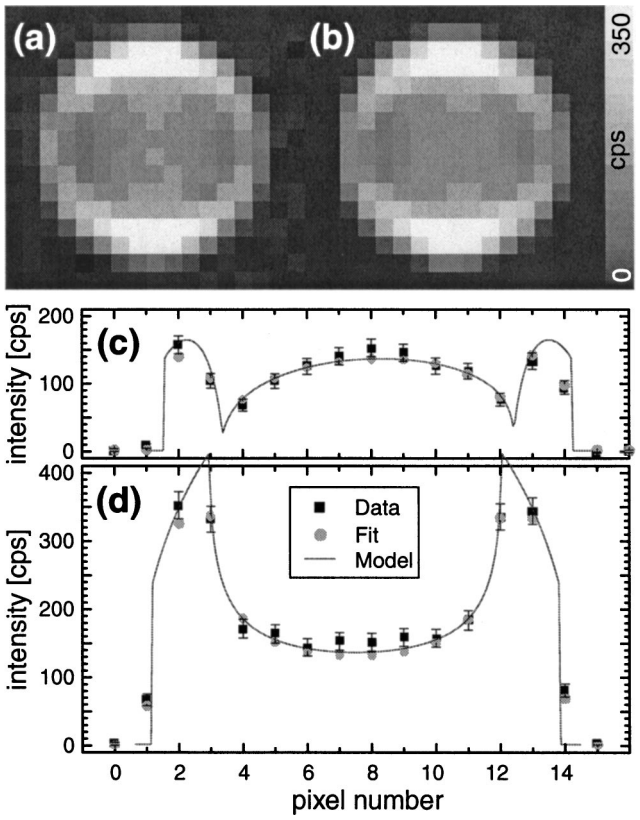

Fig. 4. Example of an observed emission pattern: (a) measured data; (b) fitted pattern; (c), (d), cross sections along a horizontal and a vertical line through the center of the pattern, respectively.

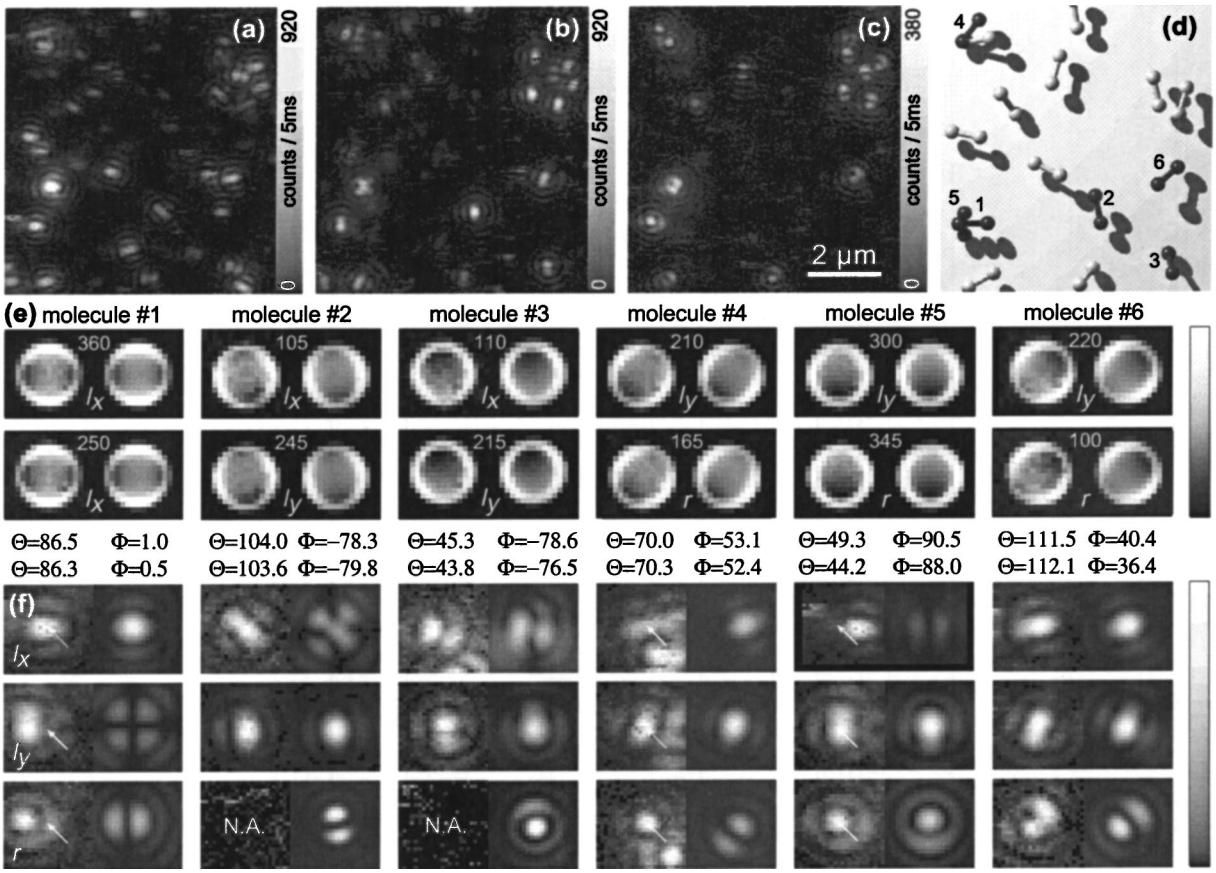

Fig. 5. Comparison of the orientations of emission dipoles and absorption dipoles: (a)–(c) Fluorescence-rate images recorded by the raster scanning of a single-molecule sample in the focal plane of a strongly focused excitation beam. The excitation beam is (a) a Gaussian beam polarized in x (horizontal polarization); (b) a Gaussian beam polarized in y (vertical polarization); and (c) a radially polarized beam. (d) Orientations of 16 molecules determined from the emission patterns. (e) Emission patterns of six selected molecules [as marked in (d)] for different excitation polarizations. The left-hand images are measured data, the right-hand images are best fits. Numbers in the top centers are maximum intensities. l_x (l_y) denotes excitation with an x-polarized (y-polarized) Gaussian beam and r denotes excitation with a radially polarized beam. (f) Comparison of corresponding fluorescence-rate images extracted from (a)–(c) (left-hand images) with calculated patterns for dipole orientations as determined from the emission patterns (right-hand images). The arrows mark the centers of the molecules to watch. Note the close proximity of other molecules for molecules 1, 4, and 5. In the images marked with N.A., the molecules were already photobleached.

being in good agreement with the theory developed at the beginning of the twentieth century. However, ensemble experiments—averaging over orientations—have been published before[25] and other emission-dipole orientation determination methods have shown their (defocused) Fourier transform.[15,28]

We analyzed several emission patterns from 16 different molecules. Some of these patterns are shown in Fig. 5. Figures 5(a)–5(c) show fluorescence-rate images of the same single-molecule sample when different excitation beams are used. Figures 5(a) and 5(b) are obtained with a fundamental Gaussian laser beam polarized along the horizontal (x) direction [Fig. 5(a)] and along the vertical (y) direction [Fig. 5(b)]. A radially polarized beam[9] was used in Fig. 5(c). In the focal plane, this excitation beam produces an axially polarized (z-direction) bright center spot enclosed by a ring with the polarization pointing in radial direction. It is well suited to excite molecules with a predominant axial component.

In the next step, we measured several emission patterns of most of the molecules visible in Figs. 5(a)–5(c) and reconstructed the orientations of the emission dipoles [Fig. 5(d)]. A comparison of six different molecules is shown in Figs. 5(e) and 5(f). These molecules correspond to the labeled molecules in Fig. 5(d). Each recorded emission pattern in Fig. 5(e) is shown together with its calculated fitted pattern. The excellent agreement indicates that a high accuracy can be achieved for the dipole orientations. Figure 5(e) also shows that the emission patterns are independent of the type of excitation beam. Furthermore, as shown by the patterns of molecules 4 and 6, we are able to distinguish between molecular orientations that have mirror symmetry, i.e., between angles Θ and $\pi - \Theta$ (axial z component positive or negative). Such a distinction cannot be accomplished with the PA methods as described, for example, in Ref. 13. The determined statistical standard deviations for the determination of the polar angles derived from all emission patterns of all 16 molecules are 1.7° for Θ and 1.1° for Φ.

For the same six molecules we extracted the corresponding fluorescence-rate patterns from Figs. 5(a)–5(c) and displayed them separately in Fig. 5(f) (left-hand patterns). Using the known field distributions in the focal plane for the different excitation beams,[8,9] we calculated

the expected fluorescence-rate patterns for the determined emission-dipole orientations (right-hand patterns). For most molecules, the two patterns agree. However, some deviations can be observed that are due to the imperfection of the excitation beam. This results in deviations from the calculated fluorescence-rate patterns. As shown in the images of molecules 1 and 5, it is also more difficult to distinguish two molecules that are close to each other. Note that the time to acquire an absorption pattern (1.6 s) was even longer than that to acquire the emission pattern (1 s). However, determination of dipole orientations by use of the absorption patterns is significantly less reliable with an experimental standard deviation of 45°. Therefore the determination of emission-dipole orientations based on emission pattern imaging is more reliable than absorption-dipole imaging.[8,9] The discussed method of mapping the emission dipoles relies solely on an intrinsically perfect source (a single dipole emitter) instead of a perfect excitation. In fact, in fluorescence-rate imaging, the perfect molecule is probing the imperfect excitation spot rather than vice versa. Finally, we point out that the accuracy of absorption-dipole imaging is much more susceptible to fluorescence blinking than our method for emission-dipole imaging. The reason is that blinking affects only certain scan lines in the fluorescence images whereas in emission-dipole imaging all CCD pixels are affected in the same way.

5. DISCUSSION

An important advantage of the detection method described in this paper is its insensitivity to aberrations in the objective lens and the exact axial location of the molecule relative to it. In defocused pattern imaging (DPI),[14,15,28] the molecular dipole orientation is determined by recording the diffraction pattern near the image plane of the objective. The diffraction pattern must be recorded outside the Fraunhofer range of the beam to detect the intensity distribution indicative of the molecules orientation. Thus the exact axial location of the molecule relative to the objective is an important experimental parameter because it determines the Fresnel number of the beam illuminating the detector. The accuracy of determining best focus is limited by the depth of focus of $\pm 1/2\, n\lambda/\mathrm{NA}^2$ for an aberration-free system (where n is the refractive index and λ is the wavelength). In the presence of spherical aberration the uncertainty in focal position increases.

Additionally, the exact diffraction pattern depends on the relative path length traveled by each angular component of the dipole. Because each angular component maps to a position in the pupil of the objective lens, the wave-front aberration of the objective distorts the relative path length of each dipole component. Thus, to associate a recorded intensity pattern with a molecular orientation, DPI should include the aberration function of the imaging system, because even a small amount of aberration can distort the diffraction pattern near focus as is routinely used in the star test.[30] This aberration function is field dependent and would need to be characterized across the field of view.

In the present work, the objective acts as a collector, gathering the light from the dipole and presenting the distribution at the exit pupil of the objective. This intensity distribution is reimaged with a low NA to the imaging detector. Aberrations in the objective do not appreciatively redistribute the intensity distribution in the objective. Furthermore, the collected distribution is insensitive to both the axial and the lateral position of the molecule. Because microscope objectives operate telecentrically in object space, the angular distribution of light at the exit pupil does not translate with lateral translation. The mean wave front leaves the exit pupil slightly off axis, but will be reimaged onto the CCD detector exactly centered. Defocusing the objective relative to the molecule changes the maximum angular component accepted by the objective in the same way as changing the object position changes the working NA of the system. The change in NA versus change in axial position Δz is $\Delta\mathrm{NA} = \mathrm{NA}\,\Delta z/f$. For $\mathrm{NA} = 1.4$, $f = 2.0\,\mathrm{mm}$, $\Delta z = 0.002$ mm, the effective change in NA is $\Delta\mathrm{NA} = -0.0014$. Thus, for a change of focus that does not exceed the depth of focus of the objective lens, the change in NA is insignificant.

Simulations show that the method presented here has a uniformly distributed standard deviation of the determined orientations over all polar angles θ and agree well with the experimental results for dipoles with small out-of-plane components. However, the experimental results show a reduced accuracy of the determination of the polar angle θ for dipoles with large axial components, as can be seen for molecules 3, 5, and 6 in Fig. 5. This is most probably due to ghost images of the dipole from the various interfaces in the objective lens. This additional background intensity contributes significantly to the central part of the pattern and hampers determination of the polar angle. DPI shows a reversed trend, having reduced accuracy for mostly in-plane-oriented dipoles.[15] In this sense the two methods are complementary.

Fourkas's PA method,[13] which measures the intensities along three different polarization directions, e.g., 0°, 45°, and 90°, has a general advantage compared with that of both imaging methods: The imaging methods have contributions of dark noise or readout noise on all pixels (approximately 200), whereas PA uses only three measurements. However, in the form in which PA has been published, it is not able to determine orientations of dipoles at or near *interfaces*. This could be corrected, but it can generally not uniquely determine the polar angle Θ, i.e., orientations Θ and $\pi - \Theta$ cannot be distinguished. Nevertheless, a simulation of PA for dipoles in a *homogeneous* medium, but otherwise with the same conditions as in the experiment, has been performed. PA shows a twofold better accuracy for the orientation determination as the method presented here for polar angles Θ of approximately 45°, but a threefold decreased accuracy for polar angles Θ close to 0° or 90°, neglecting the ambiguity of its determination of Θ. This result can be explained by the fact that readout noise or dark noise on the many pixels of the imaging methods somehow averages out because of the correlations of neighboring pixels of the patterns, whereas it enters the orientation determination in full for PA. The higher uncertainties at angles θ close to 0° and 90° are due to reduced selectivity and are inherent to the method.

An advantage of PA is that the orientation determination can be easily performed on the fly. However, if the fitting is replaced with an appropriate pattern-recognition algorithm, it should be possible to perform the orientation determination by use of the imaging methods on the fly as well.

A drawback of the presented method as well as of PA is that it cannot be parallelized, whereas DPI allows parallel observation of many molecules at once. However, this results in only an extension of measurement time for the presented method and PA, which can be tolerated in most cases.

6. CONCLUSION

In summary, we showed a new, easy-to-implement method to determine dipole orientations of single molecules with high accuracy. The standard deviations of both polar angles Θ and Φ are less than 2°; however, the accuracy for large polar angles Θ is reduced in the experiment. The used time resolution of 1 s can be significantly improved if the pixel size of the acquired patterns is reduced, thereby sacrificing some of the accuracy. Further improvement can be reached by the application of an intensified CCD and by use of the information encoded in the polarization of the emitted light, i.e., use of a polarizing beam splitter and acquisition of two polarized images. We estimate that time resolutions as good as 20 ms can be reached.

Compared with DPI[15] the presented method has the advantage of being less sensitive to phase aberrations and focusing, and, compared with the PA method,[13] it has the advantage of being able to determine dipole orientations unambiguously.

ACKNOWLEDGMENTS

This research was funded by the U.S. National Science Foundation under grant BES-0086368 and the U.S. Air Force Office of Scientific Research under grant F-49620-03-1-0379, and was partially supported by the Swiss National Foundation through a fellowship for prospective researchers (MAL).

REFERENCES

1. S. Weiss, "Measuring conformational dynamics of biomolecules by single molecule fluorescence spectroscopy," Nature Struct. Biol. **7**, 724–729 (2000).
2. Ph. Tamarat, A. Maali, B. Lounis, and M. Orrit, "Ten years of single-molecule spectroscopy," J. Phys. Chem. A **104**, 1–16 (2000).
3. L. Novotny, "Single molecule fluorescence in inhomogeneous environments," Appl. Phys. Lett. **69**, 3806–3808 (1996).
4. J. Hofkens, W. Verheijen, R. Shukla, W. Dehaen, and F. C. De Schryver, "Detection of a single dendrimer macromolecule with a fluorescent dihydropyrrolopyrroledione (DPP) core embedded in a thin polystyrene polymer film," Macromolecules **31**, 4493–4497 (1998).
5. C. Tietz, F. Jelezko, U. Gerken, S. Schuler, A. Schubert, H. Rogl, and J. Wrachtrup, "Single-molecule spectroscopy on the light-harvesting complex II of higher plants," Biophys. J. **81**, 556–562 (2001).
6. L. A. Deschenes and D. A. Van den Bout, "Single-molecule studies of heterogeneous dynamics in polymer melts near the glass transition," Science **292**, 255–258 (2001).
7. J. N. Forkey, M. E. Quinlan, M. A. Shaw, J. E. T. Corrie, and Y. E. Goldman, "Three-dimensional structural dynamics of myosin V by single-molecule fluorescence polarization," Nature (London) **422**, 399–404 (2003).
8. B. Sick, B. Hecht, and L. Novotny, "Orientational imaging of single molecules by annular illumination," Phys. Rev. Lett. **85**, 4482–4485 (2000).
9. L. Novotny, M. R. Beversluis, K. S. Youngworth, and T. G. Brown, "Longitudinal field modes probed by single molecules," Phys. Rev. Lett. **86**, 5251–5254 (2001).
10. E. Betzig and R. J. Chichester, "Single molecules observed by near-field scanning optical microscopy," Science **262**, 1422–1425 (1993).
11. M. Prummer, B. Sick, B. Hecht, and U. P. Wild, "Three-dimensional optical polarization tomography of single molecules," J. Chem. Phys. **118**, 9824–9829 (2003).
12. M. Vacha and M. Kotani, "Three-dimensional orientation of single molecules observed by far- and near-field fluorescence microscopy," J. Chem. Phys. **118**, 5279–5282 (2003).
13. J. T. Fourkas, "Rapid determination of the three-dimensional orientation of single molecules," Opt. Lett. **26**, 211–213 (2001).
14. J. Sepiol, J. Jasny, J. Keller, and U. Wild, "Single molecules observed by immersion mirror objective. The orientation of Terrylene molecules via the direction of its transition dipole moment," Chem. Phys. Lett. **273**, 444–448 (1997).
15. A. P. Bartko and R. M. Dickson, "Imaging three-dimensional single molecule orientations," J. Phys. Chem. B **103**, 11237–11241 (1999).
16. A. P. Bartko and R. M. Dickson, "Three-dimensional orientations of polymer-bound single molecules," J. Phys. Chem. B **103**, 3053–3056 (1999).
17. J. D. Jackson, *Classical Electrodynamics*, 2nd ed. (Wiley, New York, 1975), Chap. 9.2.
18. A. Sommerfeld, "Über die Ausbreitung der Wellen in der drahtlosen Telegraphie," Ann. Phys. (Leipzig) **28**, 665–736 (1909).
19. H. v. Hörschelmann, "Über die Wirkungsweise des geknickten Marconischen Senders in der drahtlosen Telegraphie," Jahrbuch drahtlos. Telegr. Teleph. **5**, 14–34,188–211 (1911).
20. A. Sommerfeld, "Über die Ausbreitung der Wellen in der drahtlosen Telegraphie," Ann. Phys. (Leipzig) **81**, 1135–1153 (1926).
21. A. Sommerfeld, *Partial Differential Equations in Physics*, 5th ed. (Academic, New York, 1967).
22. H. Weyl, "Ausbreitung elektromagnetischer Wellen über einem ebenen Leiter," Ann. Phys. (Leipzig) **60**, 481–500 (1919).
23. W. Lukosz and R. E. Kunz, "Light emission by magnetic and electric dipoles close to a plane interface. I. Total radiated power," J. Opt. Soc. Am. **67**, 1607–1615 (1977).
24. E. H. Hellen and D. Axelrod, "Fluorescence emission at dielectric and metal–film interfaces," J. Opt. Soc. Am. B **4**, 337–350 (1987).
25. Ch. Fattinger and W. Lukosz, "Optical-environment-dependent lifetimes and radiation patterns of luminescent centers in very thin films," J. Lumin. **31/32**, 933–935 (1984).
26. E. Hecht, *Optics*, 4th ed. (Addison-Wesley, Reading, Mass., 2002), Chap. 4.6.2.
27. B. Hecht, D. W. Pohl, H. Heinzelmann, and L. Novotny, " 'Tunnel' near-field optical microscopy: TNOM-2," in *Photons and Local Probes*, O. Marti und R. Möller, eds., Vol. 300 of NATO Advanced Study Institute, Series E (Kluwer Academic, Dordrecht, The Netherlands, 1995), pp. 93–107.
28. M. Böhmer and J. Enderlein, "Orientation imaging of single molecules by wide-field epifluorescence microscopy," J. Opt. Soc. Am. B **20**, 554–559 (2003).
29. S. Quabis, R. Dorn, O. Glöckl, M. Reichle, and M. Eberler, "Reduction of the spot size by using a radially polarized laser beam," in *International Seminar on Novel Trends in Nonlinear Laser Spectroscopy and High-Precision Measurements in Optics*, S. N. Bagaev, V. N. Zadkov, and S. M. Arakelian, eds., Proc. SPIE **4429**, 105–111 (2001).
30. D. Malacara, *Optical Shop Testing*, 2nd ed. (Wiley-Interscience, New York, 1992), Chap. 11.